JOURNAL OF TISSUE ENGINEERING AND REGENERATIVE MEDICINE
J Tissue Eng Regen Med 2017; **11**: 1332–1342.
Published online 5 June 2015 in Wiley Online Library (wileyonlinelibrary.com) **DOI:** 10.1002/term.2031

RESEARCH ARTICLE

Treatment by Therapeutic Magnetic Resonance (TMR™) increases fibroblastic activity and keratinocyte differentiation in an *in vitro* model of 3D artificial skin

Letizia Ferroni[1], Gloria Bellin[1], Valeria Emer[1], Rosario Rizzuto[1], Maurizio Isola[2], Chiara Gardin[1] and Barbara Zavan[1]*

[1]*Department of Biomedical Sciences, University of Padova, Italy*
[2]*Dipartimenti di Medicina Animale, Produzioni e Salute (MAPS), University of Padova, Italy*

Abstract

This study investigated the effect of extremely low-frequency pulsed electromagnetic fields (PEMFs) on skin wound healing in an *in vitro* dermal-like tissue. In this study, fibroblast and endothelial cells were utilized for the *in vitro* reconstruction of dermal-like tissues treated for various times up to 21 days with PEMFs. The effects of PEMFs on cell proliferation (MTT test), cell ageing (β-galactosidase test, ROS production), gene expression, the quality of the extracellular matrix and the amount of fibroblast growth factors were analysed. The high quality of the dermis products in the presence of PEMFs at the end of the study was confirmed through the high degree of organization of keratinocytes, which were subsequently seeded on the aforementioned *in vitro* reconstructed dermis. The cells organized themselves in well-defined multi-layers and were better organized compared with the epidermis present on the dermis that was obtained without PEMF treatment. Copyright © 2015 John Wiley & Sons, Ltd.

Received 17 November 2014; Revised 3 March 2015; Accepted 21 April 2015

Keywords **artificial skin; fibroblasts; keratinocytes; wound healing; electromagnetic field**

1. Introduction

Skin is a dynamic and complex organ that relies on interactions between different cell types, biomacromolecules and signalling molecules. Injury triggers a cascade of events designed to quickly restore skin integrity (Singer and Clark, 1999). Depending on the size and severity of the wound, extensive physiological and metabolic changes can occur, resulting in impaired wound healing and increased morbidity, which causes higher death rates (Ramasastry, 2005). One of the underlying mechanisms responsible for disturbances in wound healing is an enhanced inflammatory response that causes pathological consequences, such as hypertrophic scars, keloids or chronic wounds and ulcers (Martin and Leibovich, 2005). People with diabetes are at increased risk of peripheral arterial disease and neuropathy as well as having a higher risk of developing infections and a decreased ability to clear infections (Martin, 1997; Rivera and Spencer, 2007). Therefore, people with diabetes are prone to frequent and often severe foot problems and a relatively high risk of infection, gangrene and amputation (Piaggesi *et al.*, 2003; Lobmann *et al.*, 2005). Recently, several reports have evaluated the effects of extremely low-frequency electromagnetic fields (EMFs) on tissue repair (Pesce *et al.*, 2013). In particular, the data support an anti-inflammatory effect of EMFs by modulating cytokine profiles that drive the transition from a chronic pro-inflammatory state of the healing process to an anti-inflammatory state (Gomez-Ochoa *et al.*, 2011). Molecular clarification of the mechanisms involved in the modulation of inflammatory factors following exposure to EMFs will provide a better understanding of the cellular responses induced by EMFs and provide a potential,

*Correspondence to: B. Zavan, Department of Biomedical Sciences, University of Padova, Via Ugo Bassi 58/B, Padova 35131, Italy. E-mail: barbara.zavan@unipd.it

additional treatment in non-responding, chronic wounds (Lin *et al.*, 2001). Multiple clinical studies are currently using EMFs in the healing of bone fractures (Li *et al.*, 2013; Hannemann *et al.*, 2014) and skin wounds (Aziz and Flemming, 2012; Zhao, 2009); however, little is known about the EMF mechanisms that mediate cell biology. The proliferation of fibroblasts and endothelial cells are central processes in tissue regeneration after injury (Werner *et al.*, 2007; Deonarine *et al.*, 2007). With the continued evolution of cell culture systems and the promising biological performance of three-dimensional (3D) support scaffolds, advancements have progressed rapidly in tissue engineering (Tonello *et al.*, 2003, 2005). Encouraging results were obtained with autologous keratinocyte sheets; however, these constructs were too delicate and difficult to handle (Gallico *et al.*, 1984). Researchers have turned their attention to developing composite skin substitutes in which keratinocytes are cultured on an engineered dermal layer to create an easy-to-handle and more resistant skin substitute. Different biomaterials have been used to obtain the following dermal equivalents: bovine collagen, polyglycolic acid and acellular cadaver dermis (Lu and Huang, 2013). In this context, our laboratory found significant results by co-culturing fibroblasts, endothelial cells and keratinocytes on scaffolds made from modified hyaluronic acid. Endothelial cells proliferated and organized into a microcapillary network inside a well-integrated system, and the keratinocytes were able to form well-organized networks when they were cultured on top of the system (Brun *et al.*, 1999). This system is an advantageous model to test the regenerative ability of several external cell stimulators *in vitro*. In this study, this model was used to scientifically investigate the effects of an externally applied, low-power, pulsed electromagnetic field (PEMF) on the rate of wound healing in an *in vitro* human skin model through biological, morphological and molecular analyses of the wound-healing process.

2. Materials and methods

2.1. PEMF exposure: Therapeutic Magnetic Resonance (TMR™)

The TMR device (developed by Thereson) is composed of a console that generates electrical signals and an emitter connected to the console that converts the electrical signals into pulsating magnetic fields. The emitter comprises two solenoids with 36 turns of copper wire of 0.8 mm diameter. The signal comprises a plurality of base pulses (I) grouped in pulse packets (P) and in pulse trains (Tr), in which each pulse packet consists of a series of base pulses (I) followed by a first pause (Tpac_off) in which each pulse train (Tr) consists of a series of pulse packets (P) followed by a second pause (Ttr_off). The control circuit is configured to reverse the polarity of the base pulses (I) after a given time interval. The frequency of the base pulses is 100 Hz, and the repetition frequency of the pulse packet (P) is 2.89–25.9 Hz. The repetition frequency of pulse trains (Tr) is 0.3–2.8 Hz, while the time interval is 120–180 s. The repetition frequency of the train sets is 0.1–0.3 Hz. Each base pulse (I) has a sawtooth waveform, and each base pulse (I) comprises a series of curved profiles, in such a manner that in a pulse time interval (Time_on), the waveform increases and creates a plurality of cusps. The average amplitude of the generated magnetic field is < 40 μTesla (comparable to the Earth's magnetic field). The PEMFs from the TMR were applied to the cell cultures for 24 min twice daily for up to 30 consecutive days.

2.2. Biomaterials for 3D cell cultures

Sponges and non-woven meshes made of HYAFF®11, a linear derivative of hyaluronic acid (HYA), in which the carboxylic moiety of the glucuronic acid monomer in the HYA chain is completely esterified with benzyl groups, were supplied by Fidia Advanced Biopolymers (Abano Terme, Italy). These sponges contained open interconnecting pores, and the sponges were provided as cylinders. The non-woven meshes contained 50 mm-thick fibres, and all carriers were sterilized by γ-irradiation before use. Overall, 1×1 cm^2 pieces of the HYA non-woven/sponge material were fixed to culture plates with a fibrin clot. After detachment from the culture plates, the cells were cultured in the HYA-based scaffolds at a density of 500 000/cm^2 for 21 days in a specific differentiation medium.

2.3. Cell cultures

Human keratinocytes and dermal fibroblasts were prepared according to a modified version of the protocol of Rheinwald and Green (1975). The cells were isolated from full-thickness skin biopsies (3×1 cm) obtained from five healthy female patients aged 35–45 years. The samples were harvested during breast reduction (three patients) or abdominoplasty procedures (two patients) after written informed consent had been obtained. After epithelial sheet dispase removal, the dermis was cut into small pieces (2–3 mm^2) and the fibroblasts were isolated by sequential trypsin and collagenase digestion. These cells were then cultured with Dulbecco's modified Eagle's medium (DMEM) supplemented with 10% fetal bovine serum (FBS; Bidachem, Fornovo San Giovanni Bergamo, Italy) plus 2 mM L-glutamine and 1% penicillin/streptomycin (cDMEM). The medium was changed twice a week, and the cells were harvested by trypsin treatment. Human umbilical vein endothelial cells (HUVECs) were prepared according to a modified version of the protocol of Gardin *et al.* (2012). Umbilical cords were freshly supplied by the local Obstetrics and Gynaecology Division. Briefly, after perfusion of the vein with a metal needle, the vein was rinsed twice with saline solution (PBS2; phosphate-buffered saline without Ca^{2+} and Mg^{2+}). The endothelial cells were separated from the vein walls by collagenase

DOI: 10.1002/term

type IA (Sigma, St. Louis, MO, USA) digestion (1 mg/ml; 300–400 U/mg) for 10 min at 37°C in a physiological solution. The reaction was terminated by adding complete Medium 199 (Seromed, Istanbul, Turkey; M199 plus 2 mM L-glutamine, 1% penicillin/streptomycin, 2.5 mg/ml amphotericin B, i.e. cM199) supplemented with 20% FBS without growth factors. This same medium was used for the resuspension of the cell pellet after centrifugation for 10 min at 1100 rpm and for the seeding of the cells onto collagenated plastic flasks.

Culture substrates were prepared by treating plastic dishes overnight with collagen type I solution (Sigma; 4 μg/ml). The HUVECs were expanded after detachment with 0.05% trypsin/0.02% EDTA (Seromed) and were then split at a 1:2 ratio. After the first passage, the complete culture medium was supplemented with 1 ng/ml human recombinant ECGF, 1 ng/ml human bFGF (Calbiochem, Danvers, MA, USA) and 1 mg/ml porcine heparin (Seromed). A maximum of three passages were allowed before the seeding of endothelial cells into the HYAFF scaffold.

2.3.1. Cell cultures into HYAFF scaffolds

In total, 30 1 × 2 cm^2 pieces of the HYAFF-11 non-woven material were fixed to culture plates with a fibrin clot. Human dermal fibroblasts were then seeded onto the scaffold after detachment from the culture plates. The fibroblasts were cultured for 3 weeks in 10% FBS cDMEM with freshly added 1 ng/ml bFGF and 1/250 mg/ml ascorbic acid in HYAFF-11 scaffolds at a density of 3×10^4 cells/cm^2. After reaching confluence, the HUVECs were harvested from collagenated flasks and seeded at a density of 3×10^4 cells/cm^2 in HYAFF-11 scaffolds. These were grown in the same M199 complete culture medium as described for a collagenated flask culture. To identify the influence of the stimulating factors released by the fibroblasts, HUVEC sister cultures were cultured for 3 weeks with fibroblast-conditioned medium and were harvested 3 days after fibroblast culture.

2.3.2. Endothelial dermal equivalents

Preliminarily, various ratios of the two cell populations were seeded to identify ideal conditions: 2:1, 1:1, 1:2 and 1:3 endothelial cells:fibroblasts for the HUVEC/fibroblast co-cultures. The fibroblasts and endothelial cells were then seeded onto the HYAFF-11 scaffolds at a density of 3×10^4 cells/cm^2 each (1:1 ratio). These cells were cultured for 3 weeks with M199 medium supplemented with 20% FBS and standard antibiotics. Supplementation with growth factors was omitted. All biomaterial cultures were performed in triplicate and repeated at least three times with different cell preparations. Every week, culture samples were taken and analysed for cell content as well as histological and immunohistochemical analysis.

2.3.3. Keratinocyte dermal equivalents

Keratinocytes were cultured as described above and harvested at ~80% confluence. Subsequently, these cells were seeded onto the endothelialized dermal equivalents at a density of 2×10^5 cells/cm^2 and cultured for 1 week with DMEM and Ham's F12 solution at a ratio of 3:1, and supplemented with 10% FCS, 0.4 μg/ml hydrocortisone, 5 μg/ml insulin (Sigma), 25 μg/ml adenine, 50 μg/ml ascorbic acid and antibiotics. After 1 week of submerged culture, the endothelialized skin preparations were elevated to the air–liquid interface by laying them on sterilized steel grids, 0.5 cm high, for an additional 21 days of culture. The grid pore diameter was 1 mm. All cultures were performed in triplicate and repeated at least five times with different cell preparations. Every week, the culture samples were collected for histological and immunohistochemical analyses.

2.4. Semi-quantitative analysis of cells

To analyse the endothelial cells co-cultured in the mesh scaffolds, masked microscopic examinations were performed on immunostained sections. The HUVECs were identified by CD31 receptor-monoclonal antibody immunostaining, as described. Briefly, two investigators analysed at least three slides in a blinded manner for each experiment by light microscopy, using ×20 as the initial magnification. Each slide contained three sections of the specimen, and five fields of 3 × 2 mm^2 each were analysed for each tissue section. The experiments were performed at least three times, and the values were expressed as mean ± SD.

2.5. MTT test

The cell proliferation rates were determined by the MTT (3-4,5-dimethylthiazol-2yl-2,5-diphenyltetrazolium bromide)-based cytotoxicity test, using the Denizot and Lang method with minor modifications (Gardin *et al.*, 2012). Briefly, the supernatant was gently harvested from the multi-well tissue culture plate, and 1 ml MTT solution (0.8 mg/ml in PBS) was added to the supernatant. Cultures were returned to the incubator and, after 3 h, the supernatant was harvested again. Each scaffold was then transferred to an Eppendorf microtube and 1 ml extraction solution (0.01 N HCl in isopropanol) was added. The Eppendorf microtubes were vortexed vigorously for 5 min to enable total colour release from the scaffolds, centrifuged at 14 000 rpm for 5 min and then the supernatants were read at 534 nm.

2.6. DNA content

DNA content was determined using a DNeasy Kit (Qiagen, Hilden, Germany) to isolate total DNA from the cell cultures, following the manufacturer's protocol for tissue

DOI: 10.1002/term

isolation, using overnight incubation in proteinase K (Qiagen). The DNA concentration was detected by measuring the absorbance at 260 nm in a spectrophotometer. The cell number was then determined from a standard curve (μg DNA vs cell number) generated by DNA extraction from the counted cells. The standard curve was linear over the tested range of 5–80 μg DNA ($r = 0.99$).

2.7. Senescence-associated β-galactosidase staining

β-Galactosidase staining was performed using a senescence-associated β-galactosidase (SA-β-Gal) staining kit (Cell Signaling Technology, Danvers, MA, USA) for 12 h. Briefly, human adipose-derived stem cells were cultured with 5, 10, 15 and 20 passages, with or without REAC exposure, in six-well plates (3×10^3 cells/well) for 12 h, fixed with a fixative solution, and then processed according to the kit instructions. All the experiments were repeated three times and one representative set of results is shown. The cells were then photographed under an inverted microscope at ×100 magnification for a qualitative detection of SA-β-Gal activity. The numbers of positive (blue) and negative cells were counted in five random fields under the microscope (at ×200 magnification and brightfield illumination) and the percentage of SA-β-Gal-positive cells was calculated as the number of positive cells divided by the total number of cells counted ×100.

2.8. Reactive oxygen species (ROS) measurements

The OxiSelect™ ROS Assay Kit is a cell-based assay for measuring hydroxyl, peroxyl and other ROS activity within a cell. The assay employs the cell-permeable fluorogenic probe, DCFH-DA, which diffuses into cells and is deacetylated by cellular esterases into the non-fluorescent DCFH (Figure 1). In the presence of ROS, DCFH is rapidly oxidized to highly fluorescent DCF, and the fluorescence is read on a standard fluorometric plate reader.

2.9. Real-time PCR

Total RNA was extracted using an RNeasy Lipid Tissue kit (Qiagen), including DNase digestion with the RNase-Free DNase Set (Qiagen), from the adipose tissue of the three different layers of the centrifuged lipoaspirate and from the non-centrifuged lipoaspirate samples. After the RNA yield and quality were assessed using a NanoDrop (Agilent, Santa Clara, CA, USA), 800 ng RNA was reverse-transcribed using an RT^2 First Strand Kit (Qiagen). Real-time PCR was performed according to the user's manual for the RT^2 Profiler Human Mesenchymal Stem Cells PCR array (SABiosciences, Hilden, Germany) and with RT^2 SYBR Green ROX FAST Master Mix (Qiagen). Thermal cycling and fluorescence detection were performed using a Rotor Gene Q 100 (Qiagen). PCR reactions were performed using primers at 300 nM and SYBR Green I (Invitrogen, Carlsbad, CA, USA) supplemented with 2 mM $MgCl_2$, and a programme of 40 cycles of 15 s at 95°C and 1 min at 60°C. All cDNA samples were analysed in duplicate. Fluorescence thresholds (*C*T) were determined automatically using software, with the amplification efficiencies in the range 92–110% for the analysed genes. For each cDNA sample, the *C*T of the reference gene *L30* was subtracted from the *C*T of the target sequence to obtain the *ΔC*T. The expression level was then calculated as $2^{\Delta C_T}$ and is expressed as mean ± SD of the quadruplicate samples in two separate runs. Experiments were performed using

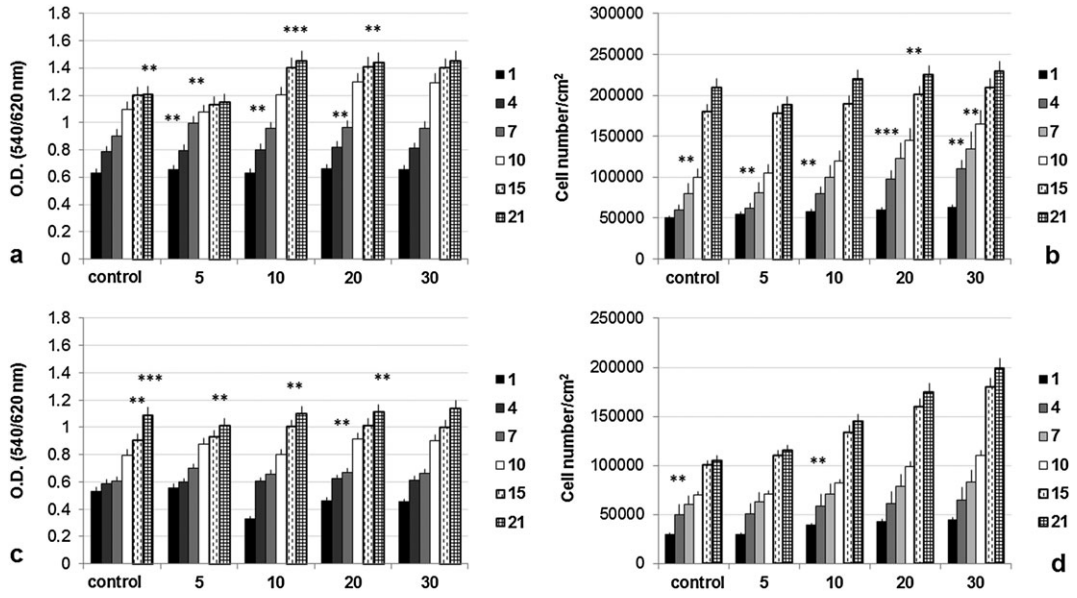

Figure 1. MTT test (a, c) and cell number/cm^2 (b, d) related to the proliferation of human fibroblasts (a, b) and HUVECs (c, d). Cells cultured in monolayers were grown for up to 21 days in the presence of a low-intensity magnetic field. Each day the cells were treated for 5, 10, 20 or 30 min with PEMFs, and proliferative activity assays were performed at fixed time points (1, 4, 7, 10, 15, or 21 days) to test cell viability: *t*-tests were used to determine significant differences ($p < 0.05$); *$p < 0.05$, **$p < 0.01$, ***$p < 0.001$

DOI: 10.1002/term

three different cell preparations and repeated at least three times. The data were analysed using Excel-based PCR Array Data Analysis Templates (SABiosciences).

2.10. Immunocytochemical and histological staining

The cellularized scaffolds were fixed in 4% paraformaldehyde phosphate-buffered saline (PBS; Seroderm, Berlin, Germany) for 72 h and then dehydrated in a graded series of ethanol and acetone (534064-500ML, Sigma Aldrich) steps. Serial 7 μm sections were cut and stained with haematoxylin and eosin (H&E) and via immunostaining. The sections were then incubated with the primary antibodies in a 2% bovine serum albumin (BSA) solution in a humidified chamber overnight at 4°C. The following primary antibodies were used: rabbit polyclonal anti-human type I collagen antibody (1:1000; AB1858, Millipore, MA, USA); rabbit polyclonal, anti-human von Willebrand factor antibody (1:100; A0082, Dako, Milan, Italy); and anti-pan-cytokeratin (1:100; C2562, Sigma). Immunofluorescence staining was performed with secondary antibody anti-rabbit IgG (H + L), which was labelled with DyLight 549 (KPL, Gaithersburg, MD, USA) and diluted 1:1000 in 2% BSA for 1 h at room temperature. Nuclear staining was performed with 2 μg/ml Hoechst H33342 (Sigma-Aldrich) solution for 2 min.

2.11. Statistical analysis

One-way analysis of variance (ANOVA) was used for data analyses. A repeated-measures ANOVA with *post hoc* analysis using Bonferroni's correction for multiple comparisons was performed, and *t*-tests were used to determine significant differences ($p < 0.05$). Repeatability was calculated as the standard deviation (SD) of the differences between measurements. All testing was performed using SPSS 16.0 software (SPSS Inc., Chicago, IL, USA; licensed by the University of Padua, Italy).

3. Results

3.1. Effects of the magnetic field on monolayered cell cultures

Human fibroblasts (Figure 1a, b) and HUVECs (Figure 1c, d) cultured in monolayers were grown for up to 21 days in the presence of a low-intensity magnetic field. Each day the cells were treated for 5, 10, 20 or 30 min with PEMFs, and proliferative activity assays were performed at fixed time points (1, 4, 7, 10, 15, and 21 days) to test cell viability. MTT tests (Figure 1a for fibroblasts; Figure 1c for endothelial cells) and DNA content tests (Figure 1b for fibroblasts; Figure 1d for endothelial cells) were performed to verify the viability of the cells in terms of mitochondrial functionality and increase in DNA production. In both cell cultures, a well-defined increase in the cell number was evident. No significant differences were present between the control (no treatment) and the cells treated with PEMFs for 5 min. Important differences were observed after 10 min of treatment, in which the presence of a magnetic field influenced cell proliferation.

3.2. Senescence-associated β-galactosidase staining

Figure 2 shows β-galactosidase staining in the fibroblasts (Figure 2a) and endothelial cells (Figure 2b) at fixed time points of 1, 4, 7, 10, 15 and 21 days that were unexposed or exposed to the electromagnetic treatment for 5, 10, 20 or 30 min. The number of SA-β-Gal-stained cells was already significantly reduced for every time point in both cell cultures that were exposed to magnetic fields when compared to the same cells left untreated, and this result became more pronounced as the culture time increased. Moreover, with a longer culture time, a remarkable increase in both the number of SA-β-Gal-positive cells and the intensity of the staining in the untreated cultures was observed.

3.3. ROS measurement

To test whether the PEMF treatment damages cell activity, we assessed ROS generation. Under environmental stress, the cells increased ROS generation, leading to an imbalance between ROS generation and its neutralization by anti-oxidative enzymes and low molecular weight anti-oxidants, such as glutathione. This disturbance in the redox equilibrium is defined as oxidative stress. Under conditions of oxidative stress, the cell accumulates ROS, and the anti-oxidative response that follows involves modifications in signalling pathways. As reported in Figure 2c (for fibroblasts) Figure 2d (for endothelial cells), a time-dependent decrease in metabolic activity was observed in cells treated with PEMF. In the controls (cells not treated with PEMFs), an increase in ROS production due to the *in vitro* ageing of the cells was observed. When the cultured cells (both fibroblasts and endothelial cells) were treated with PEMFs, a well-defined decrease in ROS production was revealed, and this finding confirms the ability of PEMFs to influence mitochondrial function.

3.4. Effects of magnetic field on *in vitro* dermal-like tissue

To verify the effects of a magnetic field on cell proliferation in an *in vitro* model similar to *in vivo* tissue, we created a dermal-like tissue that was seeded with dermal fibroblasts and HUVECs in hyaluronan-based 3D scaffolds. As reported in Figure 3a, b (control and treated groups, respectively; treatment, 15 min), the cells (black

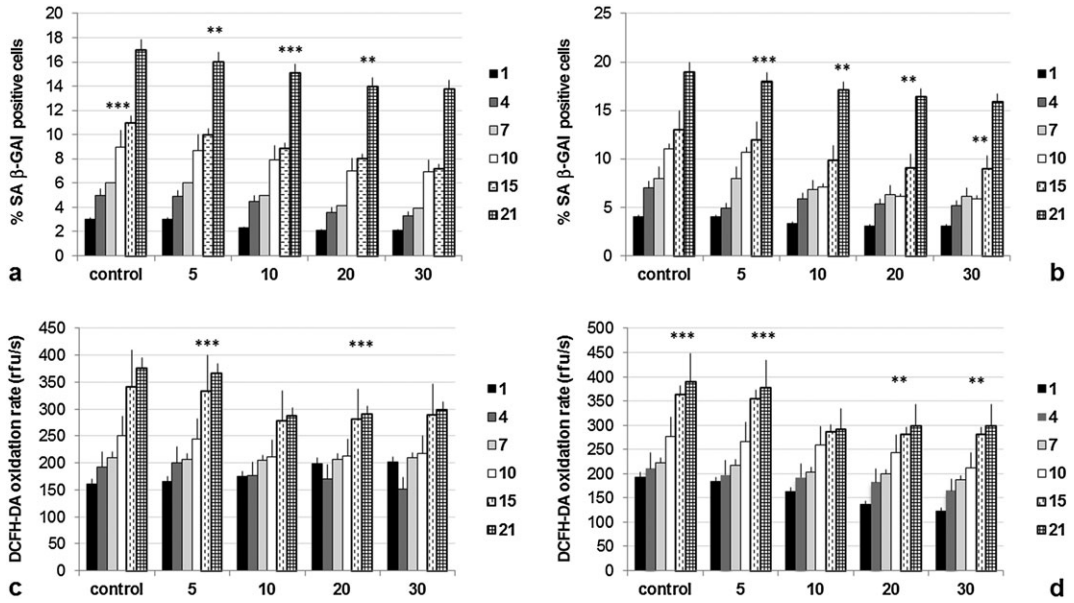

Figure 2. Senescence-associated β-galactosidase (SA β-Gal) staining in (a) fibroblasts and (b) endothelial cells, at fixed time points of 1, 4, 7, 10, 15 and 21 days, that were exposed or not to electromagnetic treatment for 5, 10, 20 or 30 min. ROS detection is reported in (c) fibroblasts and (d) endothelial cells, where a time-dependent decrease in metabolic activity was observed in cells treated with PEMF (rfu/s: relative fluorescence units/seconds). In the controls (cells not treated with PEMFs), an increase in ROS production, due to the *in vitro* ageing of the cells, was observed: *t*-tests were used to determine significant differences ($p < 0.05$); $^{*}p < 0.05$, $^{**}p < 0.01$, $^{***}p < 0.001$

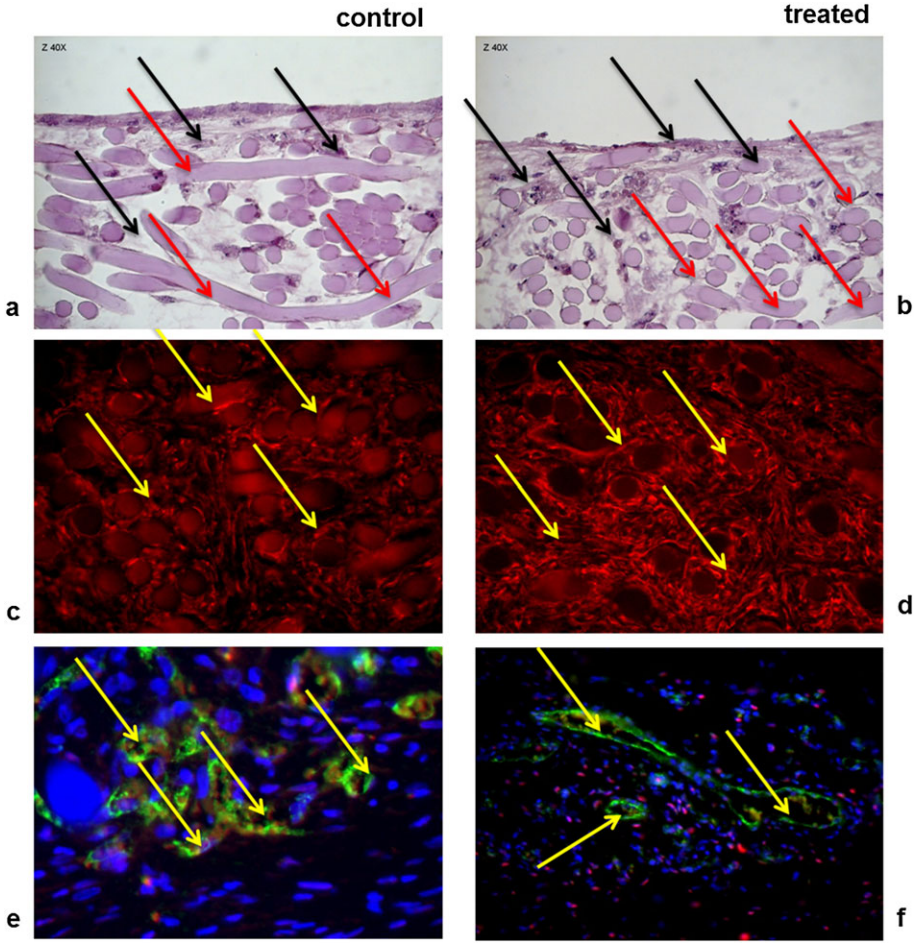

Figure 3. Morphological analyses of dermal-like tissue reconstructed *in vitro*. In (a) the control dermal-like tissue and (b) the treated dermal-like tissue, cells (black arrows) organize themselves in 3D features around the fibres (red arrows). The fibroblasts produced a well-organized extracellular matrix in (c) the control and (d) the treated group, as shown by the presence of red fibres (positive reaction of collagen type I staining, yellow arrows). Endothelial cells were present in the dermal-like tissue in both the (e) treated and (f) control groups and grew inside the scaffolds, adhered to the extracellular matrix and maintained their differentiated phenotype, as shown by the positive reaction to CD31 (coloured red and indicated by yellow arrows). [Colour figure can be viewed at wileyonlinelibrary.com]

DOI: 10.1002/term

arrows) filled the scaffolds, grew inside the scaffolds and organize themselves in 3D features around the fibres (red arrows). The fibroblasts produced a well-organized extracellular matrix (ECM) (Figure 3c, d; control and treated groups, respectively), either in the interstices or around the fibres of the scaffolds in both groups, as shown by the presence of red fibres (positive reaction of collagen type I staining; yellow arrows).

Endothelial cells were present in the dermal-like tissue in both the treated and control groups (Figure 3e, f) and grew inside of the scaffolds, adhered to the ECM and maintained their differentiated phenotype, as shown by the positive reaction to CD31 (marker for endothelial cells, coloured red and indicated by yellow arrows). Histological analysis revealed an enhanced distribution of endothelial cells inside the scaffolds during the magnetic treatment of the cultures. CD 31-positive cells were the organized HUVECs in long bundles that, in several cases, produced microcapillary structures in which a lumen was delimited. To better quantify this observation, biological and molecular analyses were performed.

The proliferation rate, which was determined by the MTT test (Figure 4a), showed an increase in the proliferative activity of the 3D cell cultures. No difference in the proliferative activity was observed in a 5 min treatment; however, an increase in the proliferation rate was observed after the 10 min treatments.

To analyse the activity and distribution of the endothelial cells, we performed a semi-quantitative cell count of the immunostained HUVECs and haematoxylin-stained fibroblasts. The proliferation rate of the HUVECs was time-dependent and increased between weeks 1 to 3 for both conditions. A larger increase in the cell number was more pronounced when the cells were in the presence of a magnetic field for a longer period of time (15 min) (Figure 4b).

The expression of genes involved in the wound-healing process was analysed to determine which gene was more sensitive to the presence of a magnetic field. Several genes of proteins involved in dermis development were analysed: for ECM composition, collagen type 1 (*COL1A1*) collagen type 2 (*Col1A2*), collagen type 3 (*COL3A1*), collagen type IV (*COL4A1*), collagen type V (*COL5A1*); vitronectin; for cellular adhesion, epithelial cadherine (CDH1); for integrins a1, -2, -3, -4, -5, -6 and -v (*ITGA1*, *ITGA2*, *ITGA3*, *ITGA4*, *ITGA5*, *ITGA6* and *ITGAV*) and b1, -3, -5 and -6 (*ITGB1*, *ITGB3*, *ITGB5* and *ITGB6*); for stemness ability, *WNT*; and for growth factors, fibroblast growth factor 2, -7 and -10 (*FGF2*, *FGF7* and *FGF10*), platelet-derived growth factor-A (*PDGFA*), transforming growth factor-A and -B (*TGFA* and *TGFB1*). In all the genes studied, a well-defined increase in their expression levels was evident for three genes related to the fibroblast growth factor family (*FGF2*, *FGF7* and *FGF 10*), for three different types of collagen (*COL4A1*, *COL5A1* and *COL3A1*), for Wnt family involved in mesenchymal stem cell commitment, and one gene, vitronectin, that is involved in fibroblast cell adhesion. As reported in Figure 5, *FGF7* showed the most significant variation in in the absence and presence of a magnetic field.

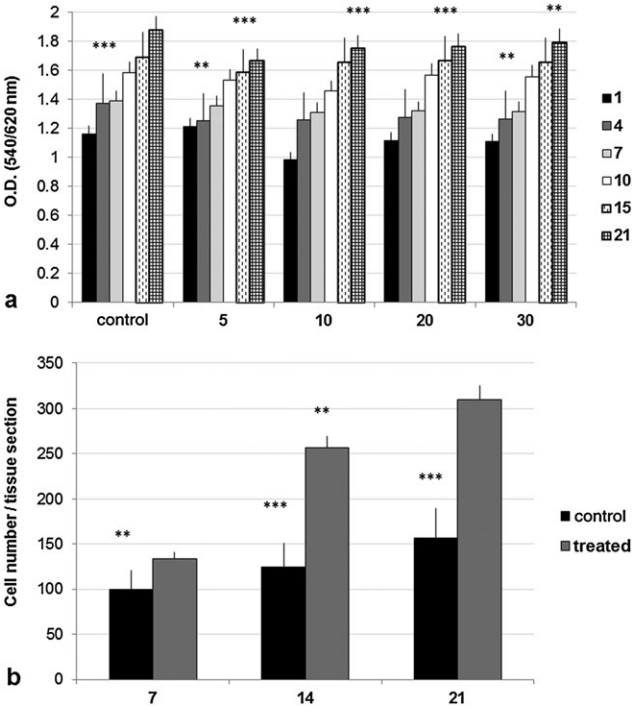

Figure 4. (a) The proliferation rate, through MTT test in 3D cell cultures, determined by the MTT test in the absence and presence of a magnetic field for a longer period of time. The proliferation rate showed an increase in the proliferative activity of the 3D cell cultures. No difference in the proliferative activity was observed in a 5 min treatment; however, an increase in the proliferation rate was observed after the 10 min treatments. (b) Activity of PEMF on endothelial cells. We performed a semi-quantitative cell count of the immunostained HUVECs and haematoxylin-stained fibroblasts. The proliferation rate of the HUVECs was time-dependent and increased between weeks 1–3 for both conditions. A larger increase in the cell number was more pronounced when the cells were in the presence of a magnetic field for a longer period of time (15 min): *t*-tests were used to determine significant differences ($p < 0.05$); *$p < 0.05$, **$p < 0.01$, ***$p < 0.001$

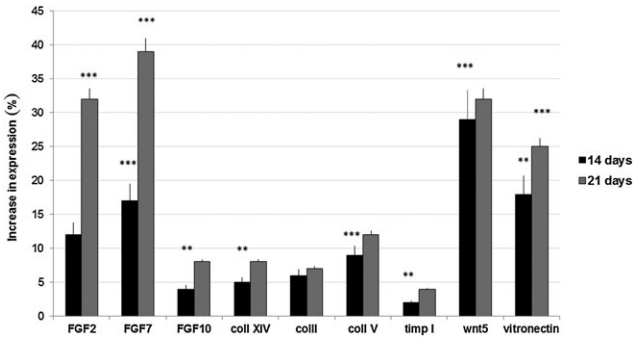

Figure 5. Gene expression of genes involved in wound healing. The expression of genes involved in the wound-healing process was analysed to determine which gene is more sensitive to the presence of a magnetic field. In total, three genes related to the fibroblast growth factor family (*FGF2*, *FGF7* and *FGF10*), three different types of collagen (collagens IV, V and III), Wnt5 involved in mesenchymal stem cell commitment and two genes involved in fibroblast cell adhesion (timp1 and vitronectin) were studied. In all the genes studied, a well-defined increase in their expression levels was evident: *t*-tests were used to determine significant differences ($p < 0.05$); *$p < 0.05$, **$p < 0.01$, ***$p < 0.001$

3.5. Effect on the dermis stimulated with PEMFs in the organization of keratinocytes

A 3D dermis that was grown in the presence of PEMFs was used as a support for the keratinocyte culture, to determine whether this substrate influences the reconstruction of the epidermis. Keratinocytes were isolated and seeded on either the dermis, with or without the PEMF treatment, and cultured for up to 14 days in semi-immersion conditions to stimulate the keratinization process. Immunohistological analysis for pan-cytokeratin was performed to verify the 3D organization of the obtained epidermis. As reported in Figure 6, keratinocytes (in green, yellow arrow) in either the presence or absence of PEMFs grew on a dermis enriched with collagen type I (red staining, red arrows). The organization of the cells was markedly different. Specifically, in the absence of PEMFs (Figure 6a, yellow circles), the cells were disorganized, while in the presence of PEMFs, keratinocytes were organized and pluristratified as in normal skin (Figure 6b). The morphology of the cells changed in the different strata, ranging from rounded-shaped cells that were present in the bottom layers to flat cells in the top layer, with a cytoplasm rich in keratin proteins.

4. Discussion

Fibroblasts are the workhorse of the most important tissue that holds the human body together – connective tissue. Connective tissue joins and supports all other tissues, including the parenchymal tissues of organs. This connective tissue is made of fibroblasts, widely spaced in a vast ECM of fibrous proteins and gelatinous ground substance. Fibroblasts produce the ECM's structural proteins (e.g. fibrous collagen and elastin), adhesive proteins (e.g. laminin and fibronectin) and ground substance (e.g. glycosaminoglycans, such as hyaluronan and glycoproteins). However, fibroblasts also play various additional roles beyond ECM production. For example, fibroblasts serve pivotal roles in ECM maintenance and reabsorption, inflammation, angiogenesis, cancer progression and in physiological as well as pathological tissue fibrosis and wound healing (fibroblasts in wounds). With regard to this latter activity, ECM proteins have been shown to play an integral role in a dynamic relationship between fibroblasts, stem/progenitor and other reparative cell populations, growth factors and matrix modifying-enzymes (ECM stem cells). It is widely accepted that the ECM plays a key role in tissue repair, beyond its ability to provide a structural framework for cells, through its ability to modulate cell behaviour. Novel technology directed at promoting ECM development in terms of quality and quantity during the course of wound repair will provide novel strategies for the treatment of pathological healing of the skin.

In this context, wound repair stimulation is one of the stronger and better documented biological effects of PEMFs. Encouraging results have been suggested by several studies *in vitro* (Athanasios *et al.*, 2007; Cossarizza *et al.*, 1993), using rats and mice (Patiño *et al.*, 1996; Bouzarjomehri *et al.*, 2000; Ushiyama and Ohkubo, 2004). Human clinical studies have highlighted that PEMFs act in reducing healing time and the rate of recurrence of venous leg ulcers (Callaghan *et al.*, 2008). In particular, Cañedo-Dorantes *et al.* (2002) observed that exposure to PEMFs induced a significant decrease in wound depth and pain intensity in patients with venous ulcers, and none of the patients treated exhibited a worsening of the lesions. Additionally, patients exposed to PEMFs demonstrated a significantly higher rate of healing of venous leg ulcers and protection from ulcer recurrence when compared with the control group (Mulder *et al.*, 2014). Cañedo-Dorantes *et al.* (2002) reported that field exposure of venous aetiology ulcers reduced or eliminated pain, oedema and weeping up to 6 weeks after the

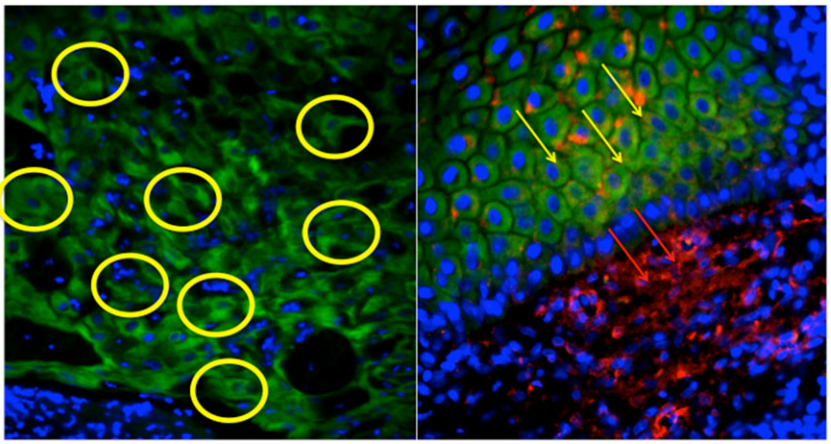

Figure 6. Morphological analyses of *in vitro* reconstructed 3D epidermis before and after the treatment. A 3D dermis that was grown in the presence of PEMFs was used as a support for the keratinocyte culture. Immunohistological analysis for pan-cytokeratin was performed to verify the 3D organization of the obtained epidermis. Keratinocytes (in green, yellow arrow) in either the presence or the absence of PEMFs grew on a dermis enriched with collagen type I (red staining, red arrows). The organization of the cells was markedly different. Specifically, in the absence of PEMFs (a) the cells were disorganized, while in the presence of PEMFs (b) the keratinocytes were organized and pluristratified, as in normal skin. [Colour figure can be viewed at wileyonlinelibrary.com]

DOI: 10.1002/term

initiation of the therapy. However, a more recent study (Ventura, 2013) showed no benefits, suggesting the need to more accurately determine the appropriate parameters for electromagnetic fields in tissue repair.

Thus, in the present study, we have tested whether a time-dependent correlation exists between the treatment with PEMF and ECM production through its effect on cell behaviour. First, we tested the effect of PEMFs in fibroblasts and endothelial cell monolayer cultures. These two types of cell population were identified as the principal actors involved in the ECM composition during the wound-healing process: fibroblasts are involved in the production of a novel ECM, and endothelial cells are involved in the formation of granulation tissue and the development of new vessels. The results confirmed that a minimum treatment of 10 min was sufficient to induce a well-defined increase in the cell proliferation of both cell cultures. The ageing process related to the long-term *in vitro* cultures was also strongly influenced by PEMF treatment. A slow-down in the ageing process was also closely associated with the PEMF treatment time, with the minimum treatment time being 10 min. Moreover, this treatment does not exert a negative effect on mitocondrial homeostasis, as shown by a decrease in ROS production related to environmental stress on the mitochondria.

In order to analyse the activity on 3D ECM composition, we applied the same PEMF treatment to an *in vitro* model of capillary-enriched skin that was basically a reconstruction of the *in vivo* setting. Biomaterial made from modified hyaluronic acid (HYAFF-11), which had already been successfully used in skin (Brun *et al.*, 1999), cartilage (Brun *et al.*, 2008) and adipose tissue engineering (Clauser *et al.*, 2014), was used for the *in vitro* reconstruction of the endothelialized dermis substitutes. Using these HYAFF-11 scaffolds, two different human cell types (fibroblasts and endothelial cells) were seeded and grown. Initially, the fibroblasts were seeded to allow for the production of the primary ECM molecules necessary for the proliferation and differentiation of endothelial cells. As reported in Figure 3a–d, and has been demonstrated in previous papers (Zavan *et al.*, 2005; Carraro *et al.*, 2010; Bressan *et al.*, 2012), fibroblasts secrete both structural and adhesive molecules, such as type I, III, IV and VII collagens, laminin-1 and -5 and fibronectin, into the interstices of the 3D scaffolds.

Our *in vitro* dermal-like engineered tissue demonstrated that the seeding of the fibroblasts and endothelial cells into the same hyaluronan-based scaffolds gave rise to a composite culture in which the fibroblasts produced the main extracellular molecules, while the endothelial cells easily proliferated and organized themselves into microcapillary-like structures (Figure 3e, f).

Tissue was obtained that had been treated with PEMFs at the same intensity and time as the monolayer cultures. Histological analysis of endothelialized dermis stained with H&E demonstrated that cultured cells were organized into dermal tissue compartments (Figure 3a, b). Inside the scaffold, a great population of fibroblasts is evident (Figure 4a, black arrows) and, as reported in Figure 4, PEMF treatment improved the vitality of the cells in 3D culture and also influenced the increase in the number of endothelial cells (Figure 5, related to MTT test and cell counting). Moreover, a detailed analysis of the gene expression related to the principal molecules involved in ECM development demonstrated a well-defined increase in collagen and *FGF* gene expression in the presence of PEMFs. In detail, we found that PEMF treatment influenced the increase in production of structural proteins, such as collagen (collagens IV, V and III), increased the adhesion ability of fibroblasts through vitronectin, and increased the paracrine activity of fibroblasts through increasing gene expression of several fibroblast growth factors, such as *FGF2*, *FGF7* and *FGF10*. As reported in Figure 5, *FGF7* showed the most significant variation in the absence and presence of a magnetic field. Fibroblasts were distributed both on top of and within the 3D constructs and were able to produce adhesive ECM molecules (as shown by real-time PCR, reported in Figure 5) and structural proteins, such as collagen type I, as revealed by immunostaining (Figure 4c, d, yellow arrows).

The good quality of this new dermis was confirmed by the positive influence of this tissue on keratinocyte organization. As it is well reported in Figure 6, keratinocytes, which need an excellent feeder layer for growth and differentiate in pluristratified multilayers, are able to organize in a well-structured epidermis tissue only in presence of a dermal-like tissue obtained after PEMF treatment. The good influence on endothelial cells has been also detected by immunostaining, as reported in Figure 3c, d, where flattened cells resembling endothelial cells adhered to the biomaterial fibres and delimited the ring structures in the dermal layer (yellow arrows, green staining in Figure 3e, f). CD31 staining of endothelialized skin constructs demonstrated that endothelial cells seeded onto the dermal equivalent had, after 30 days of culture, adhered and proliferated along the entire surface of the dermal layer and begun to infiltrate within the scaffold structure. Subsequently, the endothelial cells migrated, forming capillary-like ring structures in the newly synthesized ECM. Moreover, in the interstitial spaces of the scaffold, endothelial cells were organized into ring aggregates, similar to capillary structures, in which a lumen was clearly evident (Figure 3f). Figure 6b illustrates the thickening epithelial layer and progressive differentiation of keratinocytes. After 30 days of co-culture at the air–liquid interface, the epithelial layer became progressively stratiform, with a basal layer including cuboid perpendicularly orientated cells, a superficial layer of flattened cells and a stratum corneum provided by longitudinally aligned cells clearly evident (Figure 6b). Immunohistochemical characterization with anti-pan-cytokeratin antibody, a well-documented marker of the keratinocyte phenotype, confirmed the progressive proliferation and differentiation of the epidermal layer (Figure 6b). In the absence of PEMF treatment, keratinocytes are not able to differentiate and maintain a cuboid phenotype (yellow circles) without any strata formation. ECM molecules secreted by fibroblasts provide the physiological environment needed for endothelial and keratinocytes cell proliferation and organization into skin-like structures.

DOI: 10.1002/term

A well-orchestrated basic skin structure was here generated in the presence of PEMF treatment, in which a differentiated epidermal layer covered an underlying endothelialized dermal structure.

In conclusion, the results of this study suggest that exposure to a pulsed magnetic field influences the biology of the cells involved in ECM secretion and organization, supporting the idea that magnetic fields influence the physiology of the human body. With these results, we confirm that PEMF treatment stimulates early formation of connective tissue and a vascular network, early collagen synthesis and better maturation of damaged tissue. Our results support that, in the presence of PEMFs, the ageing of the cells slows, which is also demonstrated by the reduction of ROS production. Moreover, in chronic wounds, the inflammatory cycle is also sustained by the generation of a pro-oxidant microenvironment. Leukocytes and resident cells, particularly several fibroblasts that show premature senescence (Schafer and Werner, 2008), are sources of ROS (Sen and Roy, 2008; Patruno *et al.*, 2010). These molecules actively induce the expression of proinflammatory cytokines, chemokines, MMPs and serine proteases. Here, we can speculate that PEMFs exert a positive rejuvenation effect on the cells through the reduction of ROS, leading to a better wound-healing process.

Conflict of interest

The authors have declared that there is no conflict of interest.

Acknowledgements

This research was supported by a University of Padova (progetto di Ateneo) grant to B.Z.

References

Athanasios A, Karkambounas S, Batistatou A *et al.* 2007; The effect of pulsed electromagnetic fields on secondary skin wound healing: an experimental study. *Bioelectromagnetics* **28**: 362–368.

Aziz Z, Flemming K 2012; Electromagnetic therapy for treating pressure ulcers. *Cochrane Database Syst Rev* **12**: 12.

Bouzarjomehri F, Hajizadeh S, Sharafi AA, *et al*. 2000; Effects of low frequency pulsed electromagnetic fields on wound healing in rat skin. *Arch Intern Med* **3**: 23–27.

Bressan E, Ferroni L, Gardin C, *et al*. 2012; Donor age-related biological properties of human dental pulp stem cells change in nanostructured scaffolds. *PLoS One* **7**e49146. doi: 10.1371/journal.pone.0049146.

Brun P, Cortivo R, Zavan B, *et al*. 1999; *In vitro* reconstructed tisues on hyaluronan-based temporary scaffolds. *J Mater Sci Mater Med* **10**: 1–6.

Brun P, Dickinson S, Zavan B, *et al*. 2008; Characteristics of repair tissue in second- and third-look biopsies from patients treated with engineered cartilage: relationship to symptomatology and time after implantation. *Arthritis Res Therap* **10**R132. doi: 10.1186/ar2549.

Callaghan MJ, Chang EI, Seiser N, *et al*. 2008; Pulsed electromagnetic fields accelerate normal and diabetic wound healing by increasing endogenous FGF-2 release. *Plast Reconstr Surg* **121**: 130–142.

Cañedo-Dorantes L, García-Cantú R, Barrera R, *et al*. 2002; Healing of chronic arterial and venous leg ulcers through systemic effects of electromagnetic fields. *Arch Med Res* **33**: 281–289.

Carraro A, Flaibani M, Cillo U, *et al*. 2010; A combined method to enhance the *in vitro* differentiation of hepatic precursor cells. *Tissue Eng C Methods* **16**: 1543–1551. doi: 10.1371/journal.pone.0110796.

Clauser L, Ferroni L, Gardin C, *et al*. 2014; Selective augmentation of stem cell populations in structural fat grafts for maxillofacial surgery. *PLoS One* **6**e110796.

Cossarizza A, Angioni S, Petraglia F *et al*. 1993. Exposure to low frequency pulsed electromagnetic fields increases interleukin-1 and interleukin-6 production by human peripheral blood mononuclear cells. *Exp Cell Res* **204**: 385–387.

Deonarine K, Panelli MC, Stashower ME, *et al*. 2007; Gene expression profiling of cutaneous wound healing. *J Transl Med* **5**: 11.

Gallico GG, O'Connor NE, Compton CC, *et al*. 1984; Permanent coverage of large burn wounds with autologous cultured human epithelium. *N Engl J Med* **311**: 448–451.

Gardin C, Bressan E, Ferroni L *et al*. 2012; *In vitro* concurrent endothelial and osteogenic commitment of adipose-derived stem cells and their genomical analyses through CGH array: novel strategies to increase the successful engraftment of a tissue engineered bone grafts. *Stem Cells Dev* **21**: 767–777.

Gomez-Ochoa I, Gomez-Ochoa P, Gomez-Casal F, *et al*. 2011; Pulsed electromagnetic fields decrease proinflammatory cytokine secretion (IL-1β and TNFα) on human fibroblast-like cell culture. *Rheumatol Int* **31**: 1283–1289.

Hannemann PF, Mommers EH, Schots JP, *et al*. 2014; The effects of low-intensity pulsed ultrasound and pulsed electromagnetic fields bone growth stimulation in acute fractures: a systematic review and meta-analysis of randomized controlled trials. *Arch Orthop Trauma Surg* **134**: 1093–1106.

Li S, Yu B, Zhou D *et al*. 2013; Electromagnetic fields for treating osteoarthritis. *Cochrane Database Syst Rev* **14**: 1–48.

Lin H, Blank M, Rossol-Haseroth K, *et al*. 2001; Regulating genes with electromagnetic response elements. *J Cell Biochem* **81**: 143–148.

Lobmann R, Schultz G, Lehnert H 2005; Proteases and the diabetic foot syndrome: mechanisms and therapeutic implications. *Diabetes Care* **28**: 461–471.

Lu G, Huang S 2013; Bioengineered skin substitutes: key elements and novel design for biomedical applications. *Int Wound J* **10**: 365–371.

Martin P, Leibovich SJ 2005; Inflammatory cells during wound repair: the good, the bad and the ugly. *Trends Cell Biol* **15**: 599–607.

Martin P 1997; Wound healing – aiming for perfect skin regeneration. *Science* **276**: 75–81.

Mulder G, Tenenhaus M, D'Souza GF 2014; Reduction of diabetic foot ulcer healing times through use of advanced treatment modalities. *Int J Low Extrem Wounds* **13**: 335–346.

Patiño O, Grana D, Bolgiani A, *et al*. 1996; Pulsed electromagnetic fields in experimental cutaneous wound healing in rats. *J Burn Care Rehabil* **17**: 528–531.

Patruno A, Amerio P, Pesce M, *et al*. 2010; Extremely low frequency electromagnetic fields modulate expression of inducible nitric oxide synthase, endothelial nitric oxide synthase and cyclooxygenase-2 in the human keratinocyte cell line HaCat: potential therapeutic effects in wound healing. *Br J Dermatol* **162**: 258–266.

Pesce M, Patruno A, Speranza L, *et al*. 2013; Extremely low frequency electromagnetic field and wound healing: implication of cytokines as biological mediators. *Eur Cytokine Netw* **24**: 1–10.

Piaggesi A, Viacava P, Rizzo L, *et al*. 2003; Semiquantitative analysis of the histopathological features of the neuropathic foot ulcer: effects of pressure relief. *Diabetes Care* **26**: 3123–3128.

Ramasastry SS 2005; Acute wounds. *Clin Plast Surg* **32**: 195–208.

Rheinwald JG, Green H 1975; Serial cultivation of strains of human epidermal keratinocytes: the formation of keratinizing colonies from single cells. *Cell* **6**: 331–344.

Rivera AE, Spencer JM 2007; Clinical aspects of full-thickness wound healing. *Clin Dermatol* **25**: 39–48.

Schafer M, Werner S 2008; Oxidative stress in normal and impaired wound repair. *Pharmacol Res* **58**: 165–171.

Sen CK, Roy S 2008; Redox signals in wound healing. *Biochim Biophys Acta* **1780**: 1348–1361.
Singer AJ, Clark RAF 1999; Cutaneous wound healing. *N Engl J Med* **341**: 738–746.
Tonello C, Vindigni V, Zavan B, *et al*. 2005; *In vitro* reconstruction of an endothelialized skin substitute provided with a microcapillary network using biopolymer scaffolds. *FASEB J* **19**: 1546–1548.
Tonello C, Zavan B, Cortivo CE, *et al*. 2003; *In vitro* reconstruction of a human capillary-like network in on hyaluronan-based temporary scaffolds. *Biomaterials* **24**: 1205–1211.
Ushiyama A, Ohkubo C 2004; Acute effects of low-frequency electromagnetic fields on leukocyte–endothelial interactions *in vivo*. *In Vivo* **18**: 125–132.
Ventura C 2013; Tuning stem cell fate with physical energies. *Cytotherapy* **15**: 1441–1443.
Werner S, Krieg T, Smola H 2007; Keratinocyte–fibroblast interactions in wound healing. *J Invest Dermatol* **127**: 998–1008.
Zavan B, Brun P, Vindigni V, *et al*. 2005; Extracellular matrix-enriched polymeric scaffolds as a substrate for hepatocyte cultures: *in vitro* and *in vivo* studies. *Biomaterials* **26**: 7038–7045.
Zhao M 2009; Electrical fields in wound healing – an overriding signal that directs cell migration. *Semin Cell Dev Biol* **20**: 674–682.

DOI: 10.1002/term